JPE 17-5-3

https://doi.org/10.6113/JPE.2017.17.5.1150
ISSN(Print): 1598-2092 / ISSN(Online): 2093-4718

Full Bridge Resonant Inverter Using Asymmetrical Control with Resonant-frequency Tracking for Ultrasonic Cleaning Applications

Jirapong Jittakort*, Anawach Sangswang†, Sumate Naetiladdanon*, Chayant Koompai*, and Saichol Chudjuarjeen**

*,†Department of Electrical Engineering, Faculty of Engineering, King Mongkut's University of Technology Thonburi, Bangkok, Thailand
**Department of Electrical and Telecommunication Engineering, Faculty of Engineering, Rajamangala University of Technology Krungthep, Bangkok, Thailand

Abstract

Flexibility in the power control of ultrasonic transducers has remained a challenge for cleaning applications. This paper introduces a modification of the existing piezoelectric ceramic transducer (PCT) circuit to increase the range of operation through its impedance characteristics. The output power is controlled using the asymmetrical voltage-cancellation (AVC) method. Together with a phase-locked loop control, the switching frequency of the inverter is automatically adjusted to maintain a lagging phase angle under load-parameter variations during the cleaning process. With the proposed modification, the region of the zero-voltage switching (ZVS) operation is extended, which results in a wider range of output power control. A hardware prototype is constructed and the control algorithm is implemented using an STM32F4 microcontroller. Simulation and experimental results are provided to verify the proposed method for a 50-W PCT. The operating frequency and output power ranges under study are 37 - 41 kHz and 15.8 - 50 W, respectively.

Key words: Asymmetrical control, Resonant inverter, Ultrasonic cleaner

I. INTRODUCTION

Ultrasonic technology is a well-known technique to convert electrical energy into mechanical energy using ultrasonic piezoelectric ceramic transducers (PCTs). Examples of ultrasonic applications include medical equipment for muscle pain therapy, polymer ultrasound, welding devices, motors, piezoelectric transformers, transducers, and cleaners [1]-[18]. Ultrasonic cleaners have gained popularity in the contaminant cleaning of valuables such as jewelry, glasses, contact lenses, and watches. The key advantages of ultrasonic cleaners are their high capability in remove contaminants without damage, rapid time for the cleaning process, and environmental friendliness. In most ultrasonic applications, high-frequency resonant inverters are among the preferred choices for drivers. Common inverter topologies include the current-source inverter (CSI) [4]-[6] and the voltage-source inverter (VSI) [7]-[18]. A full-bridge inverter with an LC filter is used to generate a high frequency sinusoidal voltage [7]-[10], where the switching frequency is operated above the resonant frequency to maintain ZVS operation. However, these inverters, without the aid of resonant-frequency tracking capability, may suffer from hard switching operation due to load-parameter variations during practical operations. The phase-locked loop (PLL) method has been adopted for resonant frequency tracking under different operating conditions [11]-[14].

An automatic resonance-frequency tracking based on the compensated-static capacitance broadband method was proposed in [15] to improve the resonance-frequency tracking of a high quality factor resonant load. This method

Manuscript received Nov. 21, 2016; accepted Jun. 1, 2017
Recommended for publication by Associate Editor Chun-An Cheng.
†Corresponding Author: anawach.san@kmutt.ac.th
Tel: +662-470-9041, Fax: +662-470-9033, KMUTT
*Dept. of Electrical Eng., Faculty of Eng., King Mongkut's Univ. of Tech. Thonburi, Thailand
**Dept. of Electrical and Telecommun. Eng., Faculty of Eng., Rajamangala University of Technology Krungthep, Thailand

is based on the compensation of the parallel capacitor while tracking the resonant frequency. However, the controller is rather complicated for practical implementation. Output power control capability is an important part of the ultrasonic applications. A varied switching frequency method has been proposed to adjust the output power of an ultrasonic cleaner [16]. Occasionally, the switching frequency may fall out of the desired region between the resonant and anti-resonant frequencies, which results in hard-switching operation. In [17], a combination of the pulse width modulation (PWM) and pulse frequency modulation (PFM) methods is proposed to solve the narrow range of the output power control of a piezoelectric transformer. Even though the output power is satisfactorily controlled, the system efficiency is sacrificed in the low power region. The output power variation of the piezoelectric transformer is controlled by using the phase-shift (PS) method [18]. Similar to the PFM control, this method results in a low efficiency under low output power operation. The remaining challenge in ultrasonic applications is that the inductive region of PCTs is in the range of a few kilohertz. Output power control typically relies on resonant frequency tracking. Once the load is changed due to operating condition variations, the resonant frequency tracking to avoid hard switching operation is rather difficult. In other applications, such as induction heating, where similar systems with series resonant inverters are used, several switching techniques have been proposed with output power control capability under ZVS operation. An asymmetrical duty-cycle (ADC) with a fixed-switching frequency technique that employs unequal-cycle operation of the switches in a full-bridge inverter was proposed in [19]. The use of AVC has been reported with a fixed-switching frequency control strategy [20]-[22]. The AVC method exhibits superior efficiency when compared with the ADC method. It is suitable for low quality factor resonant loads. However, the output power control remains a challenge due to variations of the parameters in the resonant load during the heating process.

This paper presents an efficient power control method for the resonant inverters of the ultrasonic cleaning applications. The output power is controlled using the AVC technique. Load parameter variations of the PCT are addressed using a phase-locked loop method while maintaining ZVS operation. The inclusion of an external series inductor is proposed to extend the operating range and to amplify the output current to a desired level. The proposed series inductor serves two purposes. On the one hand, the inductive behavior of the load is extended and the ZVS operating region is increased. The flexibility of the output power control of the inverter is improved, while operating without turn-on switching loss. On the other hand, an inherent benefit of the integrated inductor is short-circuit protection capability in the case of a short in the capacitors of the PCT. A voltage-source inverter is chosen in this work to avoid the requirement of additional blocking

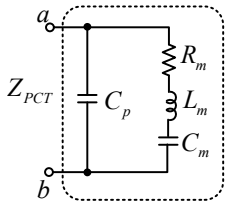

Fig. 1. Equivalent circuit of a PCT.

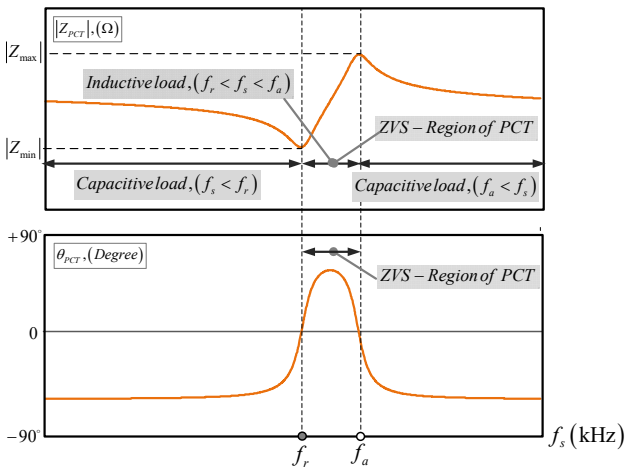

Fig. 2. Characteristic curves of $|Z_{PCT}|$ and θ_{PCT}.

diodes for the current-source inverter, a commonly used topology for PCT applications. AVC control is adopted and frequency control is proposed to mitigate the phase shift problem. This paper is organized as follows. The characteristics of PCTs are described in Section II. Section III presents the system configuration with an external series inductor and its design. An AVC method is proposed in Section IV. Simulation and experimental results are discussed in Section V. Finally, some conclusions are reported in Section VI.

II. The Piezoelectric Ceramic Transducer

An equivalent circuit of a PCT is shown in Fig. 1. It consists of a parallel capacitor (C_p) and a series combination of a resistor (R_m), an inductor (L_m) and a capacitor (C_m), representing a mechanical vibration. This particular circuit configuration is commonly referred to as a *CCL* circuit. The equivalent series impedance is varied throughout its operation depending on the load conditions such as the types and volumes of the cleaning solutions and cleaning loads. The resonant frequency (f_r) of the PCT is given as:

$$f_r = \frac{1}{2\pi\sqrt{L_m C_m}} \tag{1}$$

and the anti-resonant frequency is:

$$f_a = \frac{1}{2\pi\sqrt{L_m\left(\frac{C_m C_p}{C_m + C_p}\right)}}. \tag{2}$$

The total impedance (Z_{PCT}), resistance of Z_{PCT} (R_{PCT}), and reactance of Z_{PCT} (X_{PCT}) are expressed by:

$$\left.\begin{aligned} Z_{PCT} &= \left(\frac{\left(C_m L_m \omega^2 - 1\right) - j\omega R_m C_m}{R_m C_m C_p \omega^2 + j\left(C_m L_m C_p \omega^3 - \left(C_m + C_p\right)\omega\right)} \right) \\ R_{PCT} &= \frac{R_m C_m^2 \left(1 + C_p \left(L_m - 1\right)\omega^2\right)}{C_p^2 - 2C_m C_p \left(C_p \omega^2 - 1\right) + C_m^2 \left(1 - 2C_p \omega^2 + C_p^2 \omega^2 \left(R_m^2 + \omega^2\right)\right)} \\ X_{PCT} &= \frac{R_m^2 C_p C_m^2 \omega^2 + \left(L_m C_m \omega^2 - 1\right)\left(C_m \left(C_p \omega^2 - 1\right) - C_p\right)}{R_m^2 C_p^2 C_m^2 \omega^3 + \omega\left(C_m + C_p - C_m C_p \omega^2\right)^2} \end{aligned}\right\} \quad (3)$$

where ω is the angular switching frequency in radians per second. The *CCL* circuit can be expressed by characteristic curves of the magnitude and phase of Z_{PCT}, denoted by $|Z_{PCT}|$ and θ_{PCT}, respectively, as shown in Fig. 2. $|Z_{PCT}|$ may exhibit a capacitive or inductive behavior depending on the excited frequency. If the switching frequency f_s is in the range of $f_r < f_s < f_a$, the PCT exhibits an inductive load behavior causing a lagging phase difference. As a result, ZVS operation can be obtained. If the switching frequency is not in this range, the PCT exhibits a capacitive load behavior resulting a leading phase difference as $f_s < f_r$ or $f_a < f_s$. It is worth noting that operation in the capacitive load region may cause hard switching and damage the switches. Therefore, the ZVS operation must be carefully designed by selecting f_s to be slightly greater than f_r. When f_s is located far from f_r, the output power of the PCT becomes very low due to the high value of $|Z_{PCT}|$. As mentioned previously, the operating condition of the PCT has effect on its impedance characteristic. The load parameter variation is experimentally measured through the water volume in the container where the PCT is attached. The PCT parameters are obtained using a HIOKI/3532-50 LCR analyzer with the measurement setup, as shown in Fig. 3. Table I summarizes the measurement results. With an addition of 3 liters of water, the magnitude of the total impedance is reduced by 27.1 % and the resonant frequency is reduced by 2.5 %. Fig. 4 shows the load variation effect on $|Z_{PCT}|$ and θ_{PCT}. When the water level is increased, |Zmin|, |Zmax|, f_r and f_a are decreased. Taking the water level variation into account, a power control method without f_r tracking capability may cause the inverter to operate in a non ZVS region with the turn-on switching loss as the price to pay.

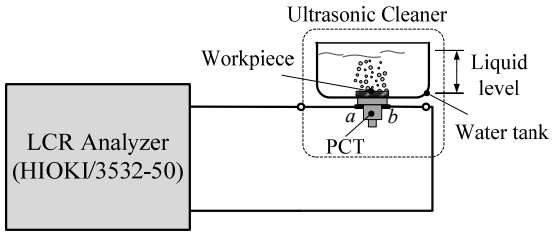

Fig. 3. Measurement setup for load variations.

TABLE I
MEASUREMENTS OF LOAD VARIATIONS

Cases	Liquid (liter)	$\|Z_{min}\|$ (kΩ)	$\|Z_{max}\|$ (kΩ)	f_r (kHz)	f_a (kHz)
(A)	None	0.480	8.80	40.05	44.00
(B)	1.5	0.454	8.15	40.00	43.95
(C)	3.0	0.350	8.05	39.10	43.90

III. *LCCL* RESONANT INVERTER TOPOLOGY

A. Proposed LCCL Circuit

The region of ZVS operation can be expanded by introducing a series inductor (L_s) to the *CCL* circuit of the PCT. The purpose of inclusion of L_s is to extend the range of ZVS operation and to amplify the output current. The advantage of this ZVS range extension is that the range of the output power control becomes greater while maintaining the lagging phase between the voltage v_{inv} and the current i_{inv} throughout the inverter operation. This enables the inverter to operate in ZVS operation and the turn-on switching loss is avoided. In addition, the inverter efficiency is improved throughout its operating range. An equivalent circuit of the proposed *LCCL* resonant circuit is simplified and shown in Fig. 5. It consists of the inverter voltage (v_{inv}), the total impedance (Z_T), and the voltage across a PCT (v_{ab}), where i_{inv}, i_o, and i_{Cp} are the inverter, output, and parallel-capacitor current, respectively. The frequency responses of the magnitude and phase of Z_T, denoted by $|Z_T(j\omega)|$ and $\theta(j\omega)$, respectively, are obtained by:

$$\left|Z_T\left(j\omega\right)\right| = \frac{\left(b_2\omega - a_2 L_s \omega^3\right) + j\left(\left(b_1 + a_3 L_s\right)\omega^3 - a_1 L_s \omega^4 - 1\right)}{\left(a_3\omega - a_1\omega^3\right) + j\omega^2 a_2} \quad (4)$$

$$\theta(j\omega) = \tan^{-1}\left(\frac{\left[\omega L_s + a_2 R_m C_m \omega^2 + \left(L_m C_m \omega^2 - 1\right)\left(C_m\left(C_p\omega^2 - 1\right) - C_p\right)\right]}{\left[a_2^2\omega^3 + \omega\left(a_3 - C_m C_p \omega^2\right)^2\right]} \times \frac{\left[C_p^2 - 2C_m C_p\left(C_p\omega^2 - 1\right) + C_m^2\left(1 - 2C_p\omega^2 + C_p^2\omega^2\left(R_m^2 + \omega^2\right)\right)\right]}{\left[R_m C_m^2\left(1 + C_p\left(L_m - 1\right)\omega^2\right)\right]} \right) \quad (5)$$

The voltage gain is given as:

$$\left|G_v\left(j\omega\right)\right| = \frac{v_{ab}}{v_{inv}} = \frac{\left(1 - b_1\omega^2\right) + j\omega b_2}{\left(L_s a_1 \omega^4 - \left(b_1 + L_s a_3\right)\omega^2 + 1\right) - j\omega^3 L_s a_2} \quad (6)$$

where $a_1=C_pC_mL_m$, $a_2=R_mC_mC_p$, $a_3=C_m+C_p$, $b_1=a_1/C_p$, and $b_2=a_2/C_p$.

To confirm the extended-ZVS range and amplified output current of the proposed method, four different sizes of L_s and various parameters of the PCT in Table II are used in the calculations of $|Z_T(j\omega)|$, $\theta(j\omega)$, and $|G_v(j\omega)|$. The effects of different values of L_s on $|Z_T(j\omega)|$, $\theta(j\omega)$, and $|G_v(j\omega)|$ are shown in Fig. 6(a)-(c), respectively. Both the $|Z_T(j\omega)|$ and $\theta(j\omega)$ responses illustrate the advantage of the inclusion of the inductor L_s. In the case of no L_s, the ZVS range is at 3.3 kHz. Since the inductor L_s is changed to 5 mH, the ZVS range has been increased to 8.8 kHz. This provides flexibility in the output power control and frequency tracking

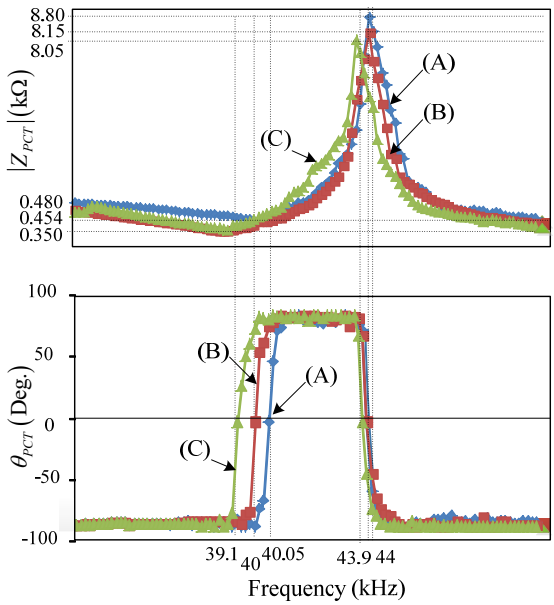

Fig. 4. Impedances $|Z|$ and phases θ under load variations.

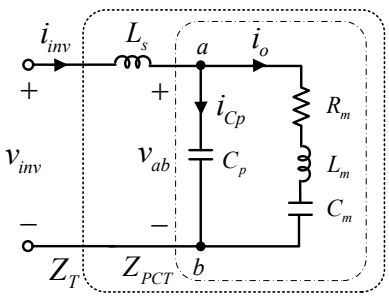

Fig. 5. The proposed equivalent circuit.

throughout the practical operating conditions. The voltage gain $|G_v(j\omega)|$ is also increased from 5 dB to 38 dB. With a proper selection of the L_s values, the desired voltage gain can be optimally chosen.

B. Design of the Series Inductor

The aim of the series inductor design is to properly ampilfy the output current and to extend the ZVS range of the *LCCL* resonant circuit. Since the switching frequency f_s is equal to f_r, the output power of the PCT, denoted by $P_{o,PCT}$, is contributed by the fundamental component current and is at its maximum value. Thus, the series impedance representing the mechanical part of the *CCL* circuit is reduced to only the resistor R_m. The RMS value of the fundamental component current i_{inv1} is obtained as:

$$I_{inv1(RMS)} = \frac{R_m - jX_{Cp}}{-jX_{Cp}}\left(\sqrt{\frac{P_{o,PCT}}{R_m}}\right). \tag{7}$$

The total impedance of the equivalent circuit is expressed as:

$$Z_T = Z_1 + jZ_{Ls} = \left(\frac{R_m}{1+\omega^2 C_p^2 R_m^2} + j\frac{\omega C_p R_m^2}{1+\omega^2 C_p^2 R_m^2}\right) + jX_{Ls} \tag{8}$$

where R_1 and X_1 are $\mathrm{Re}\{Z_1\}$ and $\mathrm{Im}\{Z_1\}$, respectively. With

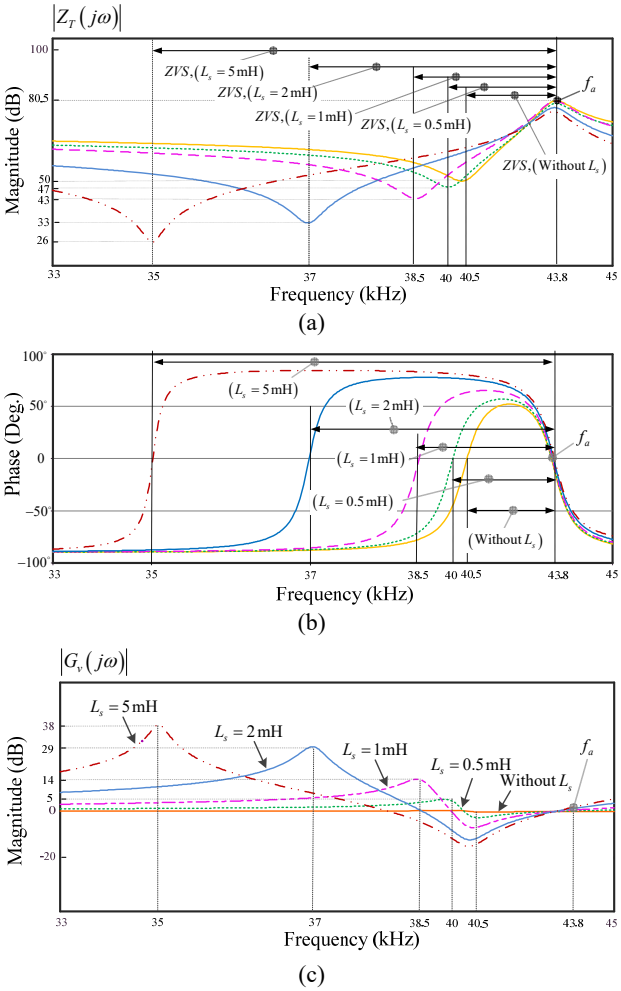

Fig. 6. Calculated results of the frequency responses: (a) $|Z_T(j\omega)|$; (b) θ; (c) $|G_v(j\omega)|$.

knowledge of the input voltage and current, the magnitude of Z_T can be determined by:

$$|Z_T| = \frac{V_{inv1,\max}}{\sqrt{2} I_{inv1(RMS)}} \tag{9}$$

where $V_{inv1,\max}$ is the amplitude of the fundamental component voltage v_{inv1}, $V_{inv1,\max} = 4V_{DC}/\pi$. From (7)-(9), the inductance L_s can be calculated by:

$$L_s = \frac{1}{\omega}\left(X_1 + \sqrt{|Z_T|^2 - R_1^2}\right). \tag{10}$$

The above inductance is used to amplify the current through the PCT to a desired level while limiting the maximum current for a specific PCT rating. The optimized value of the inductor L_s for the ultrasonic cleaner can be calculated using (10). With the parameters in Table II, the calculated inductor L_s in this study is 2 mH. The relationship in (10) can also be used in other PCTs with different ratings. For example, the designed inductor L_s for an 80 W PCT [23] has the following parameters: f_r = 80 kHz, R_m = 210 Ω, and C_p = 3.7 nF. The calculated inductance L_s is 3.75 mH. With the inclusion of the series inductor L_s, the resonant frequency of the *LCCL* circuit

TABLE II
MEASURED PARAMETERS

Parameter	Symbols	Value
Mechanical resistance	R_m	280 Ω
Mechanical inductance	L_m	18 mH
Mechanical capacitance	C_m	860 pF
Parallel capacitance	C_p	5.6 nF
Resonant frequency of Z_{PCT}	f_r	40.5 kHz
Anti-resonant frequency of Z_{PCT}	f_a	43.5 kHz
The rated power of the PCT	$P_{o,PCT}$	50 W

TABLE III
LOAD PARAMETER VARIATIONS

Cases	Series Inductor (mH)	Water (liter)	$\|Z_{min}\|$ (kΩ)	$\|Z_{max}\|$ (kΩ)	f_r (kHz)	f_a (kHz)
(1)	2	None	0.120	7.90	39.60	43.60
(2)	2	1.5	0.092	7.75	38.20	43.50
(3)	2	3.0	0.086	7.70	37.70	43.40
(4)	5	None	0.096	7.68	37.50	43.38
(5)	5	1.5	0.080	7.62	36.20	43.30
(6)	5	3.0	0.075	7.50	35.40	43.10

is slightly decreased when compared with the rated frequency of the PCT. A conduction loss due to internal resistance, and an increased system size and weight are unavoidable for the proposed series inductor L_s.

C. Effects on Load Variation

A load parameter variation during a cleaning operation is considered to illustrate the effects of the series inductor design. The liquid level and L_s values are varied. The change in the resonant frequency of the *LCCL* circuit due to variations of R_m, L_m, and C_m are observed. Table III summarizes the measurement results of load parameter variations when the liquid solvent for cleaning contaminants is distilled water.

Note that the contaminant removal depends on the vibrational effect, which is produced by vapor pressure and cavitation bubbles. In the case of a water level reduction, the vibrational effect is changed in a way that the electromechanical coupling coefficient of the vibration is effectively increased. The equivalent inductor L_m, which is inversely proportional to the square of the coupling coefficient of the vibration, is reduced, whereas the resonant frequency is increased [24]. Comparisons of the impedance $|Z|$ and the phase θ are shown in Figs. 7 and 8 with inductances L_s of 2 mH and 5 mH, respectively. For the 5 mH of L_s, the resonant frequency is decreased to 37.5 kHz with the anti-resonant frequency at 43.38 kHz in the case of no liquid solvent. This means that the ZVS operating region is around 5.5 kHz when compared with the original ZVS region of 3.95 kHz for the case with no L_s. Similarly, in the case of 3-liters of liquid solvent, the ZVS operating region has been increased from

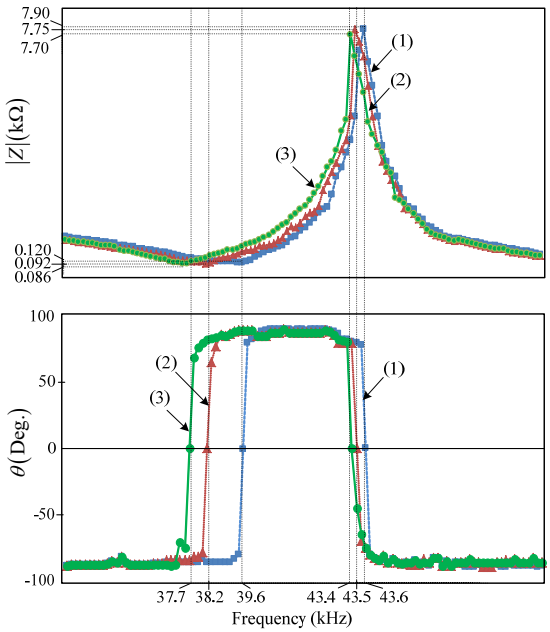

Fig. 7. Impedances $|Z|$ and phases θ for L_s = 2 mH.

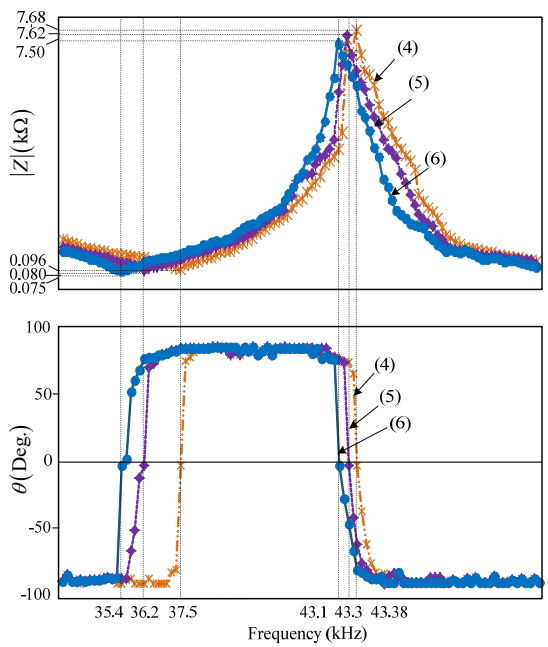

Fig. 8. Impedances $|Z|$ and phases θ for L_s = 5 mH.

4.8 kHz to 7.7 kHz. The increased ZVS operating region naturally provides flexibility in the output power control of the PCT and the resonant frequency tracking throughout the cleaning process.

IV. AVC WITH PLL CONTROL

A. Operating Principle

An inverter is used as an excitation source for the *LCCL* circuit as shown in Fig. 9. A full-wave rectifier provides a dc input voltage (V_{DC}) to the inverter. The full-bridge inverter

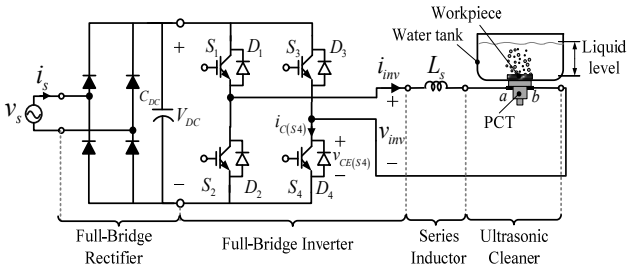

Fig. 9. Full-bridge *LCCL* resonant inverter for ultrasonic cleaners.

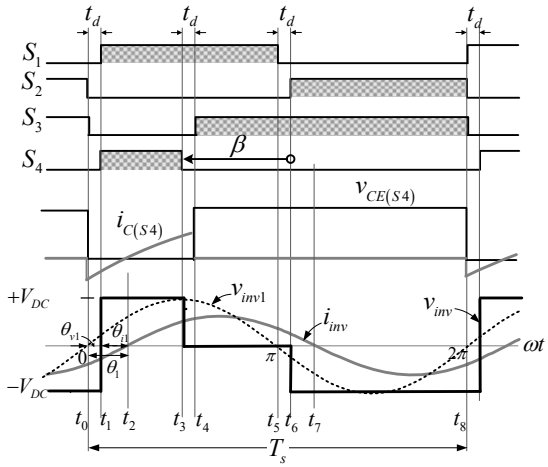

Fig. 10. Typical waveforms of the AVC technique.

consists of four IGBTs with antiparallel diodes. The *LCCL* resonant load is illustrated as a combination of the inductor L_s and the PCT. The AVC method is adopted for the output power control of the PCT. Fig. 10 shows typical waveforms of the proposed control strategy consisting of gate signals S_1-S_4, the voltage across the switch S_4 ($v_{CE(S4)}$), the current through the switch S_4 ($i_{C(S4)}$), the inverter voltage v_{inv}, the fundamental component of the inverter voltage (v_{inv1}), and the inverter current i_{inv}. The average output power (P_o) is adjusted by varying the shifting angle β through the gate signals of S_3 and S_4. The ZVS operation is achieved by setting the switching frequency f_s above the resonant frequency f_r while the inverter current i_{inv} in this stage is the same as the current $i_{C(S4)}$, lagging the input voltage v_{inv} by the phase angle of the fundamental component of the inverter current (θ_{i1}). The eight modes (t_0-t_8) of inverter operation in one switching cycle have been detailed in [22].

B. Power Calculation

The steady-state analysis of the power P_o for a full-bridge *LCCL* inverter is based on the following assumptions.

1) All of the circuit components are ideal.

2) The dc input voltage V_{DC} is constant.

3) The effects of stray capacitance and switching loss of switching devices are neglected.

The amplitude and phase components of the inverter voltage in Fig. 10 can be calculated by the following Fourier series:

$$\left.\begin{aligned}\hat{V}_{invn} &= \frac{V_{DC}}{\pi}\sqrt{a_n^2+b_n^2}\\ \theta_n &= \tan^{-1}\frac{a_n}{b_n}\end{aligned}\right\} \tag{11}$$

where, the Fourier coefficients are given as:

$$\left.\begin{aligned}a_n &= \left(V_{DC}/n\pi\right)\left[-\sin n\left(180-\beta\right)\right]\\ b_n &= \left(V_{DC}/n\pi\right)\left[2-\left(-1\right)^n-\cos n\left(180-\beta\right)\right]\end{aligned}\right\}. \tag{12}$$

Therefore, the amplitude of the fundamental voltage v_{inv1} denoted by $\hat{V}_{inv1}$ in Fig. 10 can be calculated as:

$$\hat{V}_{inv1} = \frac{V_{DC}}{\pi}\sqrt{\sin^2\left(180-\beta\right)+\left(3-\cos\left(180-\beta\right)\right)^2} \tag{13}$$

where the phase difference between the voltages v_{inv} and v_{inv1} is obtained from:

$$\theta_{v1} = \tan^{-1}\frac{\sin\left(180-\beta\right)}{3-\cos\left(180-\beta\right)}. \tag{14}$$

The amplitude and phase of the current i_{inv1} in Fig. 10 are expressed as:

$$\hat{I}_{inv1} = \frac{V_{DC}}{\pi}\frac{\sqrt{\sin^2\left(180-\beta\right)+\left(3-\cos\left(180-\beta\right)\right)^2}}{\sqrt{\left(R_{PCT}\right)^2+\left(\omega L_s+X_{PCT}\right)^2}} \tag{15}$$

and:

$$\theta_{i1} = \theta_{v1}-\tan^{-1}\left(\frac{\omega L_s+X_{PCT}}{R_{PCT}}\right). \tag{16}$$

Therefore, the output power P_o is obtained as:

$$P_o = \frac{1}{2}\hat{V}_{inv1}\hat{I}_{inv1}\cos\left(\theta_{v1}-\theta_{i1}\right). \tag{17}$$

From the above relationships, the variation of the β angle results in a change in the output power P_o. Therefore, the β angle is used to set the output power level of the PCT.

C. Output Power Control

The proposed control method is made up of two parts, namely a PLL and an AVC generator, as shown in Fig. 11. The block diagram of the PLL is used for tracking the resonant frequency. The switching frequency of the inverter is maintained slightly above the resonant frequency throughout the ultrasonic cleaning process. This enables operation in the ZVS region. The PLL control loop consists of phase detection, a low-pass filter (LPF), and a voltage controlled oscillator (VCO) unit. The PI-controller is used as a lagging phase compensator between the phase set (θ_{i1}^*) and the detected phase θ_{i1}. The PLL control loop is used for frequency control to maintain the ZVS operation. In a typical voltage-fed inverter, the gate drive signal is in phase with the asymmetrical inverter output voltage v_{inv}. A gate drive signal is often used instead of the actual load-voltage pulse for phase detection. The current signal i_{inv} is compared with the pulse output voltage signal of the VCO to detect the phase difference. The output signal of the digital phase detector is

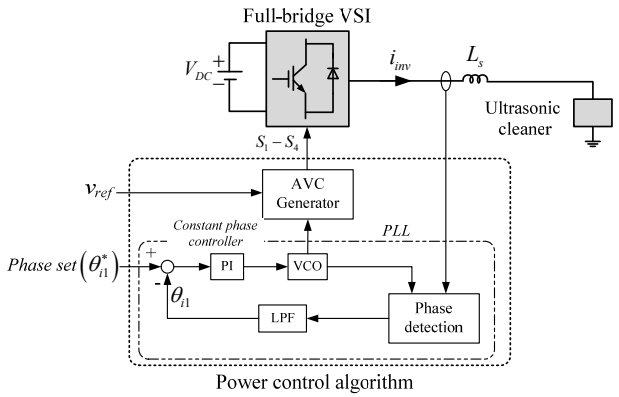

Fig. 11. Control block diagram of the proposed method.

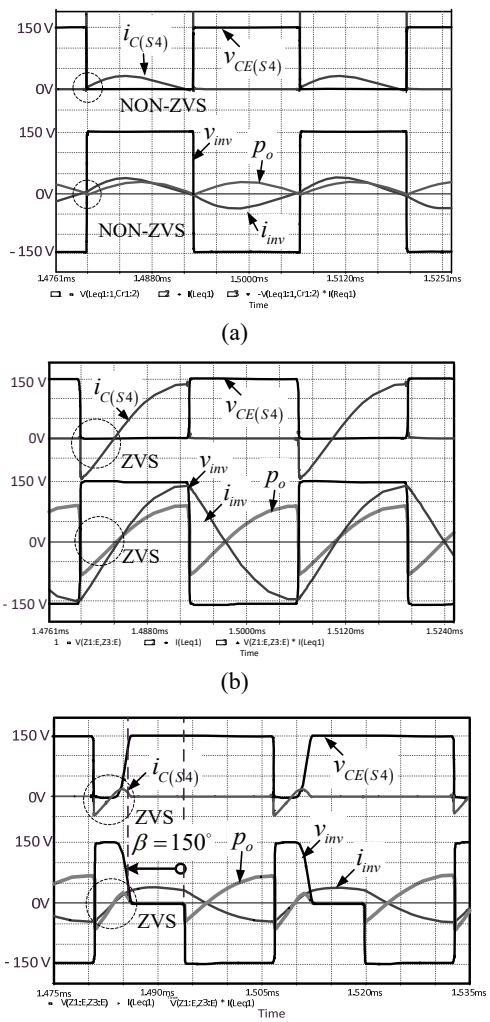

Fig. 12. Simulation results: (a) $v_{iCE(S4)}$, $i_{C(S4)}$, v_{inv}, i_{inv}, and p_o waveforms of the *CCL* load ($v_{CE(S4)}$: 50 V/div, $i_{C(S4)}$: 0.5 A/div, v_{inv}: 50 V/div, i_{inv}: 0.5 A/div, p_o: 25 W/div, time: 5 *u*s/div); (b) $v_{CE(S4)}$, $i_{C(S4)}$, v_{inv}, i_{inv}, and p_o waveforms with no phase shift under a full load of the *LCCL* load ($v_{CE(S4)}$: 50 V/div, $i_{C(S4)}$: 0.5 A/div, v_{inv}: 50 V/div, i_{inv}: 0.5 A/div, p_o: 50 W/div, time: 5 *u*s/div); (c) $v_{CE(S4)}$, $i_{C(S4)}$, v_{inv}, i_{inv}, and p_o waveforms with $\beta = 150^\circ$ at a 32% load of the *LCCL* load ($v_{CE(S4)}$: 50 V/div, $i_{C(S4)}$: 1 A/div, v_{inv}: 50 V/div, i_{inv}: 0.5 A/div, p_o: 50 W/div, time: 5 *u*s/div).

filtered by a low-pass filter to obtain an average value that is proportional to the phase difference at the load. Once the resonant frequency of the ultrasonic cleaner is changed either by a liquid level variation or additional cleaning loads, the phase difference is varied and the switching frequency is adjusted through the VCO to maintain the desired phase difference, according to the mentioned PLL algorithm. The ZVS operation is essentially enabled in all of the output power levels. The output power of the PCT is set through the reference shifting angle β_{ref}. The gate signals of the switches S_1-S_4 are constructed using a pulse-width modulation generator, where the reference voltage (v_{ref}) and the pulse signal from the VCO unit are taken as input signals.

V. Simulation and Experimental Results

To confirm the validity of the proposed topology and control method, computer simulation and hardware experimental studies are performed using the parameters in Table II. A 2-mH inductor is chosen as the inductor L_s. The DC bus voltage is set to 150 V. The liquid solvent level is at 3 liters. The cleaning loads are laboratory glassware such as small test tubes, burets, and funnels.

Simulation results of the effects of L_s and the AVC control are shown in Fig. 12. Simulation waveforms of the instantaneous output power (p_o), voltages v_{inv} and $v_{iCE(S4)}$, and currents $i_{C(S4)}$ and i_{inv} for cases without and with L_s are shown in Fig. 12(a) and 12(b), respectively. With the switching frequency fixed at 38.5 kHz, the case without L_s results in non ZVS operation since the resonant frequency is at 40.5 kHz. At this stage, the inverter suffers from the hard switching operation and turn-on switching loss. With the inclusion of the inductor L_s, the resonant frequency is moved to 37.7 kHz and ZVS operation is achieved. As found earlier, the liquid solvent level has an effect on the PCT impedance and resonant frequency. Therefore, the volume of the liquid solvent is reduced to 1.5 liters. Simulation waveforms of the power (p_o), voltages v_{inv} and $v_{iCE(S4)}$, and currents $i_{C(S4)}$ and i_{inv} of the AVC control for the output power adjustment are shown in Fig. 12(c) with the shifting angle β at 150°. The angle θ_{v1} is shifted to the left and the ZVS operation may be lost. This incidence is detected by the PLL circuit and the switching frequency is automatically increased to maintain the ZVS operation. A laboratory prototype is constructed to experimentally verify the proposed system, as shown in Fig. 13. Four gate signals are controlled using a STM32F4 microcontroller. The dead time of the gate signals, t_d, is set at 0.75 μs and the phase angle θ_{i1}^* is set at 28°. Experimental waveforms are obtained using a YOKOGAWA-D2000 digital oscilloscope, as shown in Fig. 14. Experimental waveforms of the power p_o, voltages v_{inv} and $v_{iCE(S4)}$, and currents $i_{C(S4)}$ and i_{inv} of the *CCL* load are shown in Fig. 14(a). The inverter operates under the non ZVS condition where f_s at 38.5 kHz is

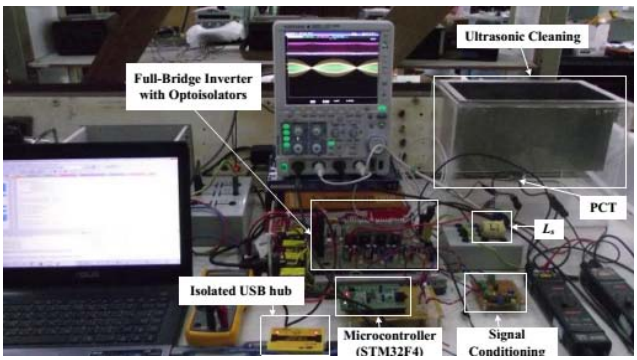

Fig. 13. Laboratory prototype of a 50-W PCT.

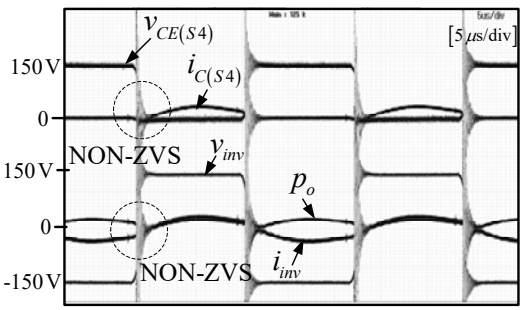

(a)

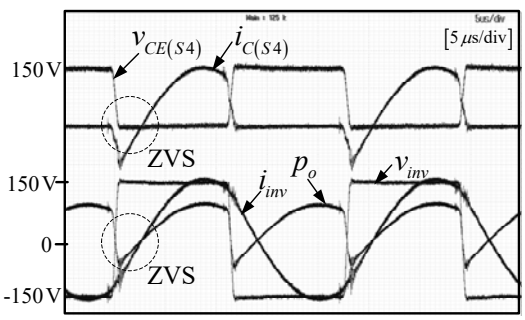

(b)

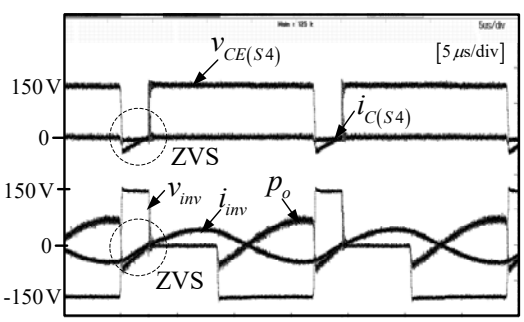

(c)

Fig. 14. Experimental results: (a) $v_{CE(S4)}$, $i_{C(S4)}$, v_{inv}, i_{inv}, and p_o waveforms of the *CCL* load ($v_{CE(S4)}$: 100 V/div, $i_{C(S4)}$: 0.5 A/div, v_{inv}: 100 V/div, i_{inv} : 0.5 A/div, p_o: 25 W/div, time: 5 *u*s/div); (b) $v_{CE(S4)}$, $i_{C(S4)}$, v_{inv}, i_{inv}, and p_o waveforms with no phase shift at the full load of the *LCCL* load ($v_{CE(S4)}$: 100 V/div, $i_{C(S4)}$: 0.5 A/div, v_{inv}: 100 V/div, i_{inv}: 0.5 A/div, p_o: 50 W/div, time: 5 *u*s/div); (c) $v_{CE(S4)}$, $i_{C(S4)}$, v_{inv}, i_{inv}, and p_o waveforms with $\beta = 150^{\circ}$ at a 32% load of the *LCCL* load ($v_{CE(S4)}$: 100 V/div, $i_{C(S4)}$: 0.5 A/div, v_{inv}: 100 V/div, i_{inv}: 1 A/div, p_o: 50 W/div, time: 5 *u*s/div).

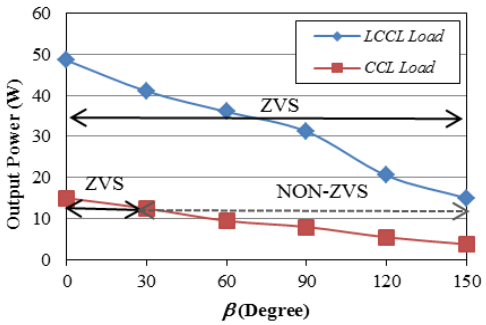

Fig. 15. Output power comparison between *CCL* and *LCCL* loads.

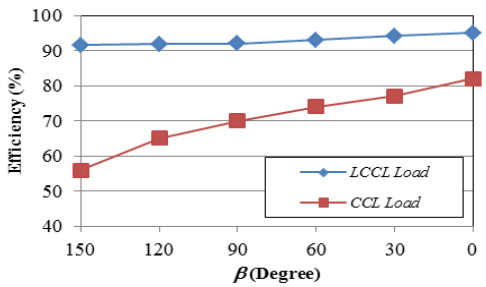

Fig. 16. Efficiency comparison between *CCL* and *LCCL* loads.

located outside the frequency range indicated in Table II. Experimental waveforms of the power p_o, voltages v_{inv} and $v_{iCE(S4)}$, and current $i_{C(S4)}$ and i_{inv} for the *LCCL* load under the full load condition ($\beta = 0^{\circ}$) are shown in Fig. 14 (b). Similar to the simulation results, the inverter is operated under the ZVS condition with the switching frequency at 38 kHz. Experimental waveforms of the power p_o, voltages v_{inv} and $v_{iCE(S4)}$, and currents $i_{C(S4)}$ and i_{inv} for the *LCCL* load for the reductions of the liquid solvent from 3 liters to 1.5 liters are shown in Fig. 14(c), where the angle β is also increased from 0° to 150°. The PLL control increases the switching frequency of the inverter to track the resonant frequency. This is to ensure the ZVS operation when the inverter operates at 38 kHz. An output comparison between the *CCL* and *LCCL* loads using the AVC method are shown in Fig. 15. With the same control, the output power of the *LCCL* load can be adjusted in the range of 15.85-49.5 W (β from 150° to 0°), while the ZVS operation is maintained. On the other hand, for the case of the *CCL* load, the ZVS operation is achieved only in the output power range of 12.5 - 15 W (β from 30° to 0°). An efficiency comparison between the *CCL* and *LCCL* loads at various values for angle β are shown in Fig. 16. The minimum efficiency of the *LCCL* load is at 91.5% when the angle β is set to 150°. When the angle β is equal to zero degrees, the efficiency is increased to 95%. The efficiency of the *CCL* load is 56% and 82% for values of angle β at 150° and 0°, respectively. The reduction in the efficiency of the *CCL* load is mainly due to the operation in the non ZVS region. The inverter suffers from turn-on switching loss in every cycle of operation. Since the switching frequency is maintained slightly above the resonant frequency, the ZVS

operation of the inverter with the proposed control scheme is guaranteed for the entire range of the variable load parameters and variable output powers.

VI. CONCLUSIONS

The inclusion of a series inductor is proposed to expand the ZVS range in the operation of inverters. The output power is controlled using the AVC control method. The presence of an additional series inductor can increase the voltage across and the current through the PCT load to the desired output power. At the same time, it can also provide inherent short circuit protection to the PCT. The PLL circuit is implemented to track the varied resonant frequency due to practical operating conditions. The system efficiency is relatively high since ultrasonic cleaners are operated under the ZVS condition throughout the cleaning process, while damage to the switches due to hard switching operation is avoided. The proposed method has been verified by simulation and experimental studies.

REFERENCES

[1] S. H. Wong, M. Kupnik, R. D. Watkins, K. Butts-Pauly, and B. T. Khuri-Yakub, "Capacitive micromachined ultrasonic transducers for therapeutic ultrasound applications," *IEEE Trans. Biomed. Eng.,* Vol. 57, No. 1, pp. 114-123, Jan. 2010.

[2] L. F. Brown, "Design considerations for piezoelectric polymer ultrasound transducers," *IEEE Trans. Ultrason., Ferroelectr., and Freq. Control,* Vol. 47, No. 6, pp. 1377-1396, Nov. 2000.

[3] L. Parrini, "Design of advanced ultrasonic transducers for welding devices," *Trans. Ultrason., Ferroelectr., and Freq. Control,* Vol. 48, No. 6, pp. 1632-1639, Nov. 2001.

[4] L. C. Cheng, Y. C. Kang, and C. L. Chen, "A resonance-frequency-tracing method for a current-fed piezoelectric transducer," *IEEE Trans. Ind. Electron.*, Vol. 61, No. 11, pp. 6031-6040, Nov. 2014.

[5] F. J. Lin, R.Y. Duan, and J. C. Yu, "An ultrasonic motor drive using a current-source parallel-resonant inverter with energy feedback," *IEEE Trans. Power Electron.*, Vol. 14, No. 1, pp. 31-42, Jan. 1999.

[6] H. Kifune and Y. Hatanaka, "A method of circuit design based on the experimental analysis of high-intensity ultrasonic transducer and the numerical analysis of zero current soft switching inverter using current overlapping commutation," in *Proc. IEEE Power Conversion*, pp. 1490-1495, 2002.

[7] N. Ghasemi, F. Zare, P. Davari, C. Langton, P. Weber, and A. Ghosh, "Power electronic converters for high power ultrasound transducers," in *Proc. IEEE ICIEA*, pp. 647-652, 2012.

[8] P. Fabijariski and R. Lagoda, "Series resonant converter with sandwich-type piezoelectric ceramic transducers," in *Proc. IEEE on Industrial Technology*, pp. 252-256, 1996.

[9] K. T. Chang, "Finding electrical transient behaviors of ultrasonic transducer in ON/OFF cycles through PSIM simulation," in *Proc. IEEE on Industrial Technology*, pp. 1121-1126, 2005.

[10] C. Winter, C. Auvigne and Y. Perriard, "Design of a resonant power inverter for a piezoelectric actuator," in *Proc. IEEE IECON*, pp.345-349, 2012.

[11] Y. K. Lo and K. J. Pai, "Feedback design of a piezoelectric transformer-based half-bridge resonant CCFL Inverter," *IEEE Trans. Ind. Electron.*, Vol. 54, No. 5, pp. 2471-2483, Oct. 2007.

[12] T. Suzuki, H. Ikeda, H. Yoshida, and S. Shinohara, "Megasonic transducer drive utilizing mosfet DC-to-RF inverter with output power of 600 W at 1 MHz," *IEEE Trans. Ind. Electron.*, Vol. 46, No. 6, pp. 1159-1173, Nov. 2014.

[13] C. Kauczor and N. Frohleke, "Inverter topologies for ultrasonic piezoelectric transducers with high mechanical Q-factor," in *Proc. IEEE PESC*, pp. 2736-2741, 2004.

[14] J. Jittakort, S. Yachiangkam, A. Sangswang, S. Naetiladdanon, S. Chudjuarjeen, and C. Koompai, "LCCL series resonant inverter for ultrasonic dispersion system with resonant frequency tracking and asymmetrical voltage cancellation control," in *Proc. IEEE IECON*, pp. 2491-2496, 2015.

[15] H. J. dong, J. Wu, G. Y. Zhang, and H. F. Wu, "An improved phase-locked loop method for automatic resonance frequency tracing based on static capacitance broadband compensation for a high-power ultrasonic transducer," *IEEE Trans. Ultrason., Ferroelectr., and Freq. Control,* Vol. 59, No. 2, 205-210, Feb. 2012.

[16] K. Agbossou, J. L. Dion, S. Carignan, M. Abdelkrim, and A. Cheriti, "Class D amplifier for a power piezoelectric load," *IEEE Trans. Ultrason., Ferroelectr., Freq. Control,* Vol. 47, No. 4, 1036-1041, Jul. 2000.

[17] S. Hamamura, T. Ninomiya, M. Yamamoto, and M. Katsuno, "Combined PWM and PFM Control for Universal Line Voltage of a Piezoelectric Transformer Off-Line Converter," *IEEE Trans. Power Electron.*, Vol. 18, No. 1, pp. 270-277, Jan. 2003.

[18] S. Nakashima, T. Ninomiya, H. Ogasawara, and H. Kakehash, "Piezoelectric-transformer inverter with maximum-efficiency tracking and dimming Control," in *Proc. IEEE APEC*, pp. 918-923, 2002.

[19] P. Imbertson and N. Mohan, "New directions in dc-dc power conversion based on idealized concepts leading ultimately to the asymmetrical duty cycle power converter," *IEEE Trans. Circuits Syst. I, Fundam. Theory Appl.*, Vol. 44, No. 8, pp. 722–727, Aug. 1997.

[20] S. Chudjuarjeen, A. Sangswang, and C. Koompai, "An improved LLC resonant inverter for induction heating applications with asymmetrical control," *IEEE Trans. Ind. Electron.*, Vol. 58, No. 7, pp. 2915-2925, Jul. 2011.

[21] S. Yachiangkam, A. Sangswang, S. Naetiladdanon, C. Koompai, and S. Chudjuarjeen, "Steady-state analysis of ZVS and NON-ZVS full bridge inverters with asymmetrical control for induction heating applications," *Journal of Power Electron.*, Vol. 7, No. 4, pp. 544-554, Mar. 2015.

[22] J. Jittakort, S. Yachiangkam, A. Sangswang, S. Naetiladdanon, C. Koompai, and S. Chudjuarjeen, "A variable-frequency asymmetrical voltage-cancellation control of series resonant inverter in domestic induction cooking," in *Proc. IEEE ICPE-ECCE Asia*, pp. 2320-2327, 2011.

[23] APC International, Ltd - https://americacanpiezo.com/images/stories/content images, April 25th 2014.

[24] Antonio. A. Vives, Piezoelectric Transducers and Application, Springer, 2008.

Jirapong Jittakort was born in Sisaket Province, Thailand, in 1974. He received his B.S. degree in Electrical Engineering from Northeastern College, Khon Kaen, Thailand, in 1996; and his M.S. degree in Electrical Engineering from King Mongkut's University of Technology Thonburi (KMUTT), Bangkok, Thailand, in 2005, where he is presently working toward his Ph.D. degree in Electrical and Computer Engineering. His current research interests include power electronics and control, high-frequency soft-switching power converters, and ultrasonic applications.

Anawach Sangswang was born in Bangkok, Thailand. He received his B.S. degree from King Mongkut's University of Technology Thonburi (KMUTT), Bangkok, Thailand, in 1995; and his M.S. and Ph.D. degrees from Drexel University, Philadelphia, PA, USA, in 1999 and 2003, respectively. He is presently working as an Assistant Professor in the Department of Electrical Engineering, KMUTT. His current research interests include stochastic modeling, the digital control of power electronic converters, and power system stability.

Sumate Naetiladdanon received his B.S. degree from Chulalongkorn University, Bangkok, Thailand, in 1995; his M.S. degree from Rensselaer Polytechnic Institute, Troy NY, USA, in 1999; and his Ph.D. degree from Osaka University, Osaka, Japan, in 2006. He is presently working as a Lecturer in the Department of Electrical Engineering of King Mongkut's University of Technology Thonburi (KMUTT), Bangkok, Thailand. His current research interests include the power electronics for power quality improvement and renewable energy.

Chayant Koompai was born in Surat Thani, Thailand. He received his B.S. degree from King Mongkut's University of Technology Thonburi (KMUTT), Bangkok, Thailand, in 1973. He has more than 30 years of experience working in the field of induction heating. His current research interests include circuit analysis and induction-heating systems.

Saichol Chudjuarjeen was born in Prachinburi, Thailand. He received his B.S. degree in Engineering from the Mahanakorn University of Technology, Bangkok, Thailand, in 2000; and his M.S. and Ph.D. degrees from King Mongkut's University of Technology Thonburi (KMUTT), Bangkok, Thailand, in 2004 and 2011, respectively. He is presently working as a Lecturer in the Department of Electrical and Telecommunication Engineering, Rajamangala University of Technology Krungthep, Bangkok, Thailand. His current research interests include high-frequency resonant inverters for induction heating, current-source and voltage-source inverters, and the control of power-electronic systems.